AIAA JOURNAL
Vol. 37, No. 12, December 1999

Quantitative Analysis of Air Convection Caused by Magnetic–Fluid Coupling

Burtsitsig Bai* and Akira Yabe†
Mechanical Engineering Laboratory, Ibaraki 305-8564, Japan
and
Jianwei Qi‡ and Nobuko I. Wakayama§
National Institute of Materials and Chemical Research, Ibaraki 305-8565, Japan

Magnetic attractive forces acting on paramagnetic oxygen have recently been found to induce gas flow and promote combustion. The study of the interaction between electrically nonconducting gases and magnetic fields is a new interdisciplinary research area called "magnetoaerodynamics." The authors present the magnetic body force acting on the gas and the governing equations for magnetoaerodynamics. The authors used these equations to evaluate the N_2–air jet numerically to understand the mechanism and physics of this phenomenon. The key results are as follows: 1) The magnetic body force becomes nonconservative under gradients of both the O_2 gas concentration and the magnetic strength. 2) The numerical analyses clarify the mechanism of the coupling between magnetic forces and the convective motion and indicate the existence of air convection and the N_2 jet due to the nonconservative magnetic body force. 3) The maximum velocity of the N_2 jet, u_{max}, increases with the magnetic strength at the center of the magnet, B_0. For $B_0 = 1.5$ T and entrance velocity of the N_2 gas of 7.4 cm/s, $u_{max} = 44$ cm/s. 4) Measured velocities were in good agreement with our simulation. This study suggests the potential use of magnetic fields to control gas flows and combustion.

Nomenclature

$\boldsymbol{B}$	= magnetic flux density
$\boldsymbol{B}_0$	= magnetic flux density at the center of the magnet
D	= diffusion coefficient
$\boldsymbol{f}_m$	= magnetic force per unit volume
$\boldsymbol{f}'_{m,i}$	= magnetic force per unit mass on species i
$\boldsymbol{H}$	= magnetic field intensity
h	= enthalpy
$\boldsymbol{j}$	= electric current density
$\boldsymbol{n}$	= unit vector normal to the surface
p	= gas pressure
$\boldsymbol{q}$	= heat-flux vector
T	= gas temperature
$\boldsymbol{u}$	= gas velocity
$\boldsymbol{V}$	= diffusion velocity vector
W_i	= molecular weight of species i
w_i	= rate of production of species i by chemical reactions
Y_i	= mass fraction of species i
λ	= thermal conductivity
μ	= magnetic permeability
μ_r	= relative magnetic permeability
μ_0	= absolute magnetic permeability of vacuum
ν	= viscosity coefficient
ρ	= gas density
σ	= stress tensor
φ_m	= magnetic potential
χ	= magnetic susceptibility per unit mass
ψ	= stream function
ω	= vorticity

Received 11 May 1998; revision received 14 June 1999; accepted for publication 15 June 1999.

*Postdoctoral Research Fellow of Japan Science and Technology, Department of Advanced Machinery; currently Special Postdoctoral Researcher, Computational Science Laboratory, Institute of Physical and Chemical Research, 2-1 Hirosawa, Wako, Saitama 351-0198, Japan.
†Director, Department of Research Planning, 1-2 Namiki, Tsukuba.
‡Postdoctoral Research Fellow of Core Research for Evolutional Science and Technology, Department of Physical Chemistry, 1-1 Higashi, Tsukuba.
§Senior Researcher, Department of Physical Chemistry, 1-1 Higashi, Tsukuba.

I. Introduction

MANY papers have reported on magnetically induced flows of electrically conducting fluids,[1] i.e., magnetohydrodynamics (MHD). However, except for the works related to ferromagnetic fluids, there have been few studies on magnetically induced flows of electrically nonconducting fluids. Recently, oxygen gas (O_2), which is paramagnetic, and air have been found to behave like magnetic fluids.[2] The paramagnetism of O_2 originates from the parallel spin of the two outer-shell electrons of an O_2 molecule,[3] and O_2 gas has a positive and large magnetic susceptibility χ. The absolute value of χ for O_2 is a few hundred times as large as that for diamagnetic gases[4] such as nitrogen (N_2), carbon dioxide (CO_2), and argon (Ar). Because of its paramagnetism, the flow of either O_2 gas or air is easily affected by magnetic fields.

Recent experimental studies[2,5,6] have shown that magnetically induced gas flows occur when gradients of both the O_2 gas concentration and the magnetic field exist. When N_2 gas is injected into air in the direction of a decreasing magnetic field, it accelerates and behaves like a jet stream,[5,6] as shown in Fig. 1a. In the absence of magnetic fields, however, N_2 gas flows very slowly (Fig. 1b). Furthermore, these magnetically induced gas flows have been found to promote combustion in diffusion flames[6] and sustain flames under microgravity conditions,[7] where such flames were otherwise found to be extinguished.[8] These phenomena are explained qualitatively by considering the magnetic attractive force acting on paramagnetic O_2 gas.

Applications of these magnetic effects hold particular promise for the control of gas flow and combustion. For example, the phenomenon shown in Fig. 1 suggests the possibility of accelerating or ventilating gas flows without a fan. However, up to now there has been no theoretical description and no quantitative evaluation of these effects. This new research area, magnetoaerodynamics, requires interdisciplinary research involving the interaction between fluids (paramagnetic and diamagnetic gases) and magnetic fields.

In this paper we present, for the first time, a theoretical description of magnetoaerodynamics and describe the magnetic body force acting on an O_2 gas mixture and the general governing equations for magnetoaerodynamics.

We use these equations to evaluate the behavior of an N_2–air jet numerically to understand the mechanism and physics of this

a) With magnetic field (B_0 = 1.5 T) b) Without magnetic field

Fig. 1 Flow visualization of the magnetically induced N_2 gas jet.

phenomenon. Furthermore, we measure the velocity profile of the N_2 gas jets to certify the accuracy of our numerical simulations.

II. Experimental Method

A gas jet, shown in Fig. 1, was obtained by introducing an N_2 gas stream into air in the direction of decreasing magnetic intensity. Figure 2 shows the experimental setup and the corresponding magnetic flux density distribution along the central y axis between the poles of an electromagnet (P). The magnetic flux density at the center of the magnet B_0 was 1.5 T. The mixture of nitrogen gas (700 ml/min) and an aqueous aerosol (0.2 g/min) was injected from a glass tube (Q) with an inner diameter of 1.6 cm. The outlet of the pipe was placed at $y = 2$ cm. An aqueous aerosol generated with an ultrasonic nebulizer (Omron NE-U11B) was added to make the flowfield visible.

A magnetic field was obtained by using an electromagnet (ISM-130WV-S, IDX Co., Ltd.). The gap of the magnet was 2 cm. The magnetic flux density was varied by changing the current through the magnet. The spatial distribution of $\boldsymbol{B}$ was measured by a Gauss meter (F. W. Bell Co., Ltd., Model 4048).

The velocity was measured with a fiberoptic laser Doppler velocimeter (LDV) (Kanomax Co., Ltd., FLV 8851). The seeding material for the LDV measurements was an aqueous aerosol. The measurement volume was $0.1\phi \times 1.1$ mm^2. The direction of the laser beam was perpendicular to the x–y plane (Fig. 2). A personal computer (Dell XPS-R450 equipped with System 8007, Kanomax) recorded the LDV signals and calculated the velocity. The velocity measurements were made in a thermally stabilized room at $T = 18$°C. To prevent disturbance from the surrounding environment, most of experimental devices were placed inside a rectangular plastic enclosure with $60 \times 40 \times 40$ cm^3.

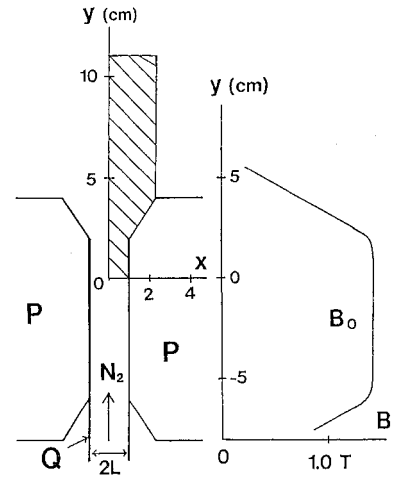

Fig. 2 Experimental setup for generating the magnetically induced N_2 gas jet shown in Fig. 1a and the spatial distribution of the magnetic flux density B along the vertical y axis: P, magnetic pole, and Q, Pyrex glass tube.

III. Theoretical Formulation

The complete mathematical formulation of magnetoaerodynamics includes the expression of the magnetic body force acting on a gas mixture as well as expressions for the mass, momentum, energy, and species conservation. In this section we describe this system of equations and apply them to magnetically induced N_2 gas flows in air to determine numerically the distributions of the magnetic flux density, fluid velocity, and gas mixture mass fractions.

A. Magnetic Body Forces

The magnetic forces acting on a fluid element can be derived from the Helmholtz free energy, which is stored in the flow medium by a magnetic field.[9–11] According to Landau and Lifshitz,[9] the magnetic

body force $\boldsymbol{f}_m$ can be expressed as [Eq. (34.3) in Ref. 9, converted to SI units]

$$\boldsymbol{f}_m = \frac{1}{2}\nabla\left[H^2\rho\left(\frac{\partial\mu}{\partial\rho}\right)_T\right] - \frac{H^2}{2}\nabla\mu + \mu[\boldsymbol{j}\times\boldsymbol{H}] \tag{1}$$

where the first term on the right-hand side (RHS) denotes magnetostriction forces caused by magnetic field gradients and the second term shows the dependence of the magnetic body force on the gradients of μ. H is the magnitude of magnetic field intensity. For electrically nonconducting fluids (i.e., $\boldsymbol{j}=0$) such as air and nitrogen gas, the third term can be neglected.

Gases are classified as either paramagnetic (PM) or diamagnetic (DM). Gases such as O_2, NO, and NO_2 are PM, whereas most other gases are DM. The magnetic permeability of gases can be expressed as follows[12]:

$$\begin{aligned} &\mu_r - 1 = \chi(T)\rho, && \mu_r = \mu/\mu_0 \\ &\chi(T) \propto T^{-1} && \text{for PM} \\ &\chi(T) \equiv \text{const.} && \text{for DM} \end{aligned} \tag{2}$$

For PM gases, this relation is known as Curie's law.

Substituting relation (2) into Eq. (1), the magnetostriction force term [first term on the RHS of Eq. (1)] becomes $\frac{1}{2}\nabla[\mu_0(\mu_r-1)H^2]$, and Eq. (1) can be rewritten as

$$\boldsymbol{f}_m = \tfrac{1}{2}\mu_0(\mu_r - 1)\nabla H^2 \tag{3}$$

For gas mixtures such as air, which include PM O_2 gas whose magnetic susceptibility is a few hundred times as large as for other DM gases, we can make the following approximation:

$$\mu_r - 1 = \sum_{i=1}^{N}\chi_i(T)Y_i\rho \approx \chi_{O_2}(T)Y_{O_2}\rho \tag{4}$$

We can then simplify the expression for $\boldsymbol{f}_m$ as

$$\boldsymbol{f}_m \approx \tfrac{1}{2}\mu_0\chi_{O_2}(T)Y_{O_2}\rho\nabla H^2 \tag{5}$$

In this work we only considered gases at room temperature. Therefore, $\chi_{O_2}(300\,\text{K}) = 107.8\times10^{-6}\ \text{cm}^3/\text{g}$ (Ref. 4).

B. General Governing Equations for Magnetoaerodynamics

The temporal and spatial distributions of ρ, $\boldsymbol{u}$, T, and Y_i in magnetoaerodynamics, including reacting flows, can be described with the following conservation and state equations.[13]

Mass conservation:

$$\frac{\partial\rho}{\partial t} + \nabla\cdot\rho\boldsymbol{u} = 0 \tag{6a}$$

Momentum conservation:

$$\frac{\partial}{\partial t}(\rho\boldsymbol{u}) + \nabla\cdot(\rho\boldsymbol{u}\boldsymbol{u}) = -\nabla p - \nabla\cdot\sigma + \boldsymbol{f}_m + \rho g \tag{6b}$$

Energy conservation:

$$\frac{\partial}{\partial t}(\rho h) + \nabla\cdot(\rho h\boldsymbol{u}) = \frac{\partial p}{\partial t} + \boldsymbol{u}\cdot\nabla p - \sigma:\nabla\boldsymbol{u} - \nabla\cdot\boldsymbol{q} + \rho\sum_i Y_i\boldsymbol{f}'_{m,i}\cdot\boldsymbol{V}_i \tag{6c}$$

Species conservation:

$$\frac{\partial}{\partial t}(\rho Y_i) + \nabla\cdot(\rho\boldsymbol{u}Y_i + \rho Y_i\boldsymbol{V}_i) = w_i \tag{6d}$$

Ideal gas law:

$$p = \rho RT\sum_i\frac{Y_i}{W_i} \tag{6e}$$

where

$$h = \sum_i h_iY_i, \qquad \sigma = \frac{2}{3}\rho\nu\nabla\cdot uU - \rho\nu\left[\nabla u + (\nabla u)^T\right]$$

Note that the magnetic force term is usually included in Eq. (6b), the momentum equation. The heat flux $\boldsymbol{q}$ and the species diffusion velocity $\boldsymbol{V}_i$ are given by Fourier's law and Fick's law.

Fourier's law:

$$\boldsymbol{q} = -\lambda\nabla T + \rho\sum_i h_iY_i\boldsymbol{V}_i$$

Fick's law:

$$\boldsymbol{V}_i = -D_i\nabla Y_i$$

Because the magnetic field is steady and there are no electrical currents, the spatial distribution of $\boldsymbol{H}$ and $\boldsymbol{B}$ are determined by Maxwell's equations as

$$\nabla\times\boldsymbol{H} = 0 \tag{7a}$$

$$\nabla\cdot\boldsymbol{B} = 0 \tag{7b}$$

$$\boldsymbol{B} = \mu\boldsymbol{H} \tag{7c}$$

In Eq. (2), μ_r is nearly equal to μ_0 because $\chi\rho \ll 1$ exists in the present gas system. Therefore, the nonuniformity of the magnetic permeability of the gas mixture would not change the magnetic field intensity distribution, and equation (7b) can become as follows:

$$\nabla\cdot\boldsymbol{H} = 0 \tag{7d}$$

Here, we define magnetic potential φ_m as

$$\boldsymbol{H} = -\nabla\varphi_m \tag{7e}$$

Then the magnetic potential φ_m satisfies the Laplace equation

$$\Delta\varphi_m = 0 \tag{8}$$

Thus, the resulting magnetic field distribution ($\boldsymbol{H}$ and $\boldsymbol{B}$) obtained from the solution of Eq. (8) is used in Eq. (5) to determine $\boldsymbol{f}_m$. Then these conservation equations can be solved numerically for a given set of initial and boundary conditions.

C. Numerical Analysis of N_2–Air Flow

In our numerical analysis of magnetically induced N_2 gas jets using Eqs. (6–8), we made the following assumptions: that they are two dimensional, that the compressibility effect is negligible, that there is isothermal flow, that there is laminar flow, and that constant viscosity and species diffusion coefficients are present.

In our experimental setup (Fig. 2), the distance between the poles of the electromagnet was about 2 cm and the depth was more than 5 cm. We, therefore, assumed that the magnetically induced gas jet was two dimensional. The assumption of incompressible flow was valid because the Mach number of this jet was below 0.2.

We used an aqueous aerosol for flow visualization but neglected its effect on the magnetic coupling with the gases because magnetic acceleration of N_2 has also been observed without seed aerosols.[6] Furthermore, we assumed that our gas flow was isothermal because we did not observe a significant difference between the temperature of the N_2 gas before and after mixing with the aerosol. Thus, we neglected the solution of the energy conservation equation.

The equations for the conservation of mass [Eq. (6a)] and momentum [Eq. (6b)] are written in terms of the stream function ψ and vorticity ω. Here, $\boldsymbol{u} = (\partial\psi/\partial y, -\partial\psi/\partial x)$ and $\omega = \nabla\times\boldsymbol{u}$.

Furthermore, to write Eqs. (5–8) in dimensionless form, L, U_M, U_M/L, H_0, and H_0L are used, respectively, as reference scales for the length, velocity, time, magnetic field intensity, and magnetic potential. H_0 is the magnetic intensity at the center of the magnet. The characteristic length L is taken as half the distance between the poles (Fig. 2). Based on dimensional analysis in the momentum conservation equation (6b), the characteristic velocity U_M is estimated by the balance between the inertial force and the magnetic force shown as follows:

$$\rho U_M^2/L = \rho\mu_0\chi_{O_2}Y_{O_2}H_0^2/L, \qquad U_M = aH_0 \tag{9a}$$

where $a = \sqrt{(0.23\mu_0\chi_{O_2})}$ and 0.23 is the mass fraction of O_2 in air.

Then we define the dimensionless parameter Re_M as the Reynolds number and the dimensionless parameter P_{eM} as the Peclet number based on U_M:

$$Re_M = U_M L/\nu = aLH_{\max}/\nu \tag{9b}$$

$$P_{eM} = U_M L/D = Re_M \nu/D \tag{9c}$$

Under these assumptions, combining Eqs. (5–8), the motion of the magnetically induced gas jet can be modeled using the following equations in dimensionless form:

$$\frac{\partial}{\partial t}\bar{\omega} + (\bar{\boldsymbol{u}}\cdot\nabla)\bar{\omega} - Re_M^{-1}\nabla^2\bar{\omega} = \frac{\partial}{\partial \bar{y}}\bar{f}_{mx} - \frac{\partial}{\partial \bar{x}}\bar{f}_{my} \tag{10a}$$

$$\nabla^2\bar{\psi} = \bar{\omega} \tag{10b}$$

$$\frac{\partial}{\partial t}Y_A + (\bar{\boldsymbol{u}}\cdot\nabla)Y_A - P_{eM}^{-1}\nabla^2 Y_A = 0 \tag{10c}$$

$$\nabla^2\Phi_m = 0 \tag{10d}$$

where

$$\{\bar{x}, \bar{y}\} = L^{-1}\{x, y\}, \qquad \{\bar{\boldsymbol{u}}\} = U_M^{-1}\{\boldsymbol{u}\}$$

$$\bar{\psi} = \psi U_M^{-1}L^{-1}, \qquad \bar{\omega} = \omega U_M^{-1}L$$

$$\bar{\boldsymbol{f}}_m = 0.23L^{-1}\mu_0\chi_{O_2}H_0^2\boldsymbol{f}_m, \qquad \Phi_m = \varphi_m L^{-1}H_0^{-1}$$

where Y_A is the mass fraction of air in the gas mixture of N_2 and air. Furthermore, $\bar{f}_{mx}$ and $\bar{f}_{my}$ are the x and y dimensionless components of $\boldsymbol{f}_m$, respectively.

The momentum equation (6b) recasts as a single equation, Eq. (10a), through eliminating the term of pressure for $\nabla\times\nabla p = 0$ in Eq. (6b). Because the flow was isothermal and the same phenomenon was also observed when N_2 gas was injected horizontally, we neglected buoyancy forces in Eq. (10a).

Figure 2 shows the calculation domain (shaded area), ranging from 0 to 2.25 cm along the x axis and from 0 to 11 cm along the y axis. Because the N_2 gas jets are symmetrical about the vertical y axis, we considered only half of the flowfield area in the simulations.

The initial conditions for the injected N_2 gas velocity profile was given as the Poiseulle velocity distribution (parabolic) with a maximum velocity of 7.4 cm/s (i.e., 700 ml/m). The boundary conditions follow in the next sections.

1. Species Concentration

$Y_A = 0$ at the inlet ($y = 0$ cm), $\partial Y_A/\partial y = 0$ at the outlet ($y =$ 11 cm), $Y_A = 1$ on the right boundary ($x = 2.25$ cm), $\partial Y_A/\partial x = 0$ on the axis of symmetry ($x = 0$ cm), and $\partial Y_A/\partial n = 0$ the surface of magnetic pole.

2. Flowfield

Here, $\partial \boldsymbol{u}/\partial x = 0$ on the axis of symmetry ($x = 0$) and the right boundary ($x = 2.25$ cm), at the inlet ($y = 0$) the velocity distribution was parabolic with a maximum velocity of 7.4 cm/s, $\partial \boldsymbol{u}/\partial y = 0$ at the outlet, and the other boundaries (the surface of the magnetic pole) were no-slip boundaries.

3. Magnetic Field

$\Phi_m = 0$ on the axis of symmetry ($x = 0$) and at the outlet, $\Phi_m = 1$ on the magnetic poles, and $\partial\Phi_m^2/\partial^2 x = 0$ on the right boundary ($x =$ 2.25 cm).

For a given set of initial and boundary conditions, Eq. (10) is then solved numerically. We used an uncoupled approach to solve Eq. (10). First, we solved for Φ_m from Eq. (10d) and determined the magnitudes of $\boldsymbol{H}$ to calculate $\boldsymbol{f}_m$ in Eq. (5), and we then solved the vorticity and species conservation equations. For the time discretization, we used the Euler explicit scheme. For the spatial discretization, we used a third-order upwind scheme[14] for the inviscid terms and a central difference scheme for the viscosity.

To overcome numerical instability, we used small time step varying between 10^{-4} and 10^{-5}. For high magnetic field strength, the smaller time step, 10^{-5}, was used.

For a typical case with $B_0 = 1.5$ T, three uniform grids of 41×41, 51×51, and 46×111 were used. The results showed for all grids the same qualitative behavior and differ quantitatively by less than 5%. Therefore, the grid of 51×51 points was used in the present computations.

D. Simulation Results and Discussion

The magnetic field intensity distribution was analyzed first to obtain the magnetic body force. For a typical case ($B_0 = 1.5$ T), the distributions of dimensionless magnetic field strength (B/B_0) along the x axis and the y axis were calculated. Figures 3a and 3b show the comparison between calculated (a solid line) and measured values along vertical axis ($x = 0$ cm) and ($x = 0.8$ cm), respectively. The calculated results shown in Fig. 3 agree with the measured values using a Gauss meter. This shows that the magnetic field distribution can be analyzed based on the constant permeability assumption.

Several parameters used in numerical simulations are shown in Table 1 with $L = 1.0$ cm, $\nu = 1.5\times 10^{-5}$ m^2 s^{-1} and $D = 0.2\times 10^{-4}$ m^2 s^{-1}. We chose this set of conditions to determine the dependence of the velocity of the N_2 gas jets on the magnetic intensity. First we present the simulation results for $B_0 = 1.5$ T, $Re_M = 498$, and $P_{eM} = 373$, which are the conditions under which the N_2 gas jet in Fig. 1a was observed.

Figures 4a–4c show the simulated distributions of Y_A, the vorticity $\bar{\omega}$, and the stream function $\bar{\psi}$, respectively, for $B_0 = 1.5$ T. Figure 4a shows a thin, long region about 7.5 cm in length along the y axis occupied by N_2 gas. Above $y = 6$ cm the region that is rich in N_2 gas spreads out to both sides, and a recirculation zone is created. These flow patterns are similar to the flow pattern shown in Fig. 1a.

Figure 4b shows that a vorticity distribution exists between the electromagnetic poles and the N_2 gas stream along the y axis. This can be understood from the governing equations of vorticity. Only when the magnetic force $\boldsymbol{f}_m$ becomes nonconservative ($\nabla\times\boldsymbol{f}_m \neq 0$) can the right-hand term in Eq. (10a) be nonzero. Thus, the magnetic force will drive air convection. In the present case, the magnetic driving force results from the gradients of the magnetic field intensity

Table 1 Simulation conditions

Parameter	Run 1	Run 2	Run 3	Run 4	Run 5
B_0, T	1.5	1.2	0.8	0.6	0.4
Re_M	498	398	266	199	133
P_{eM}	373	249	199	149	99

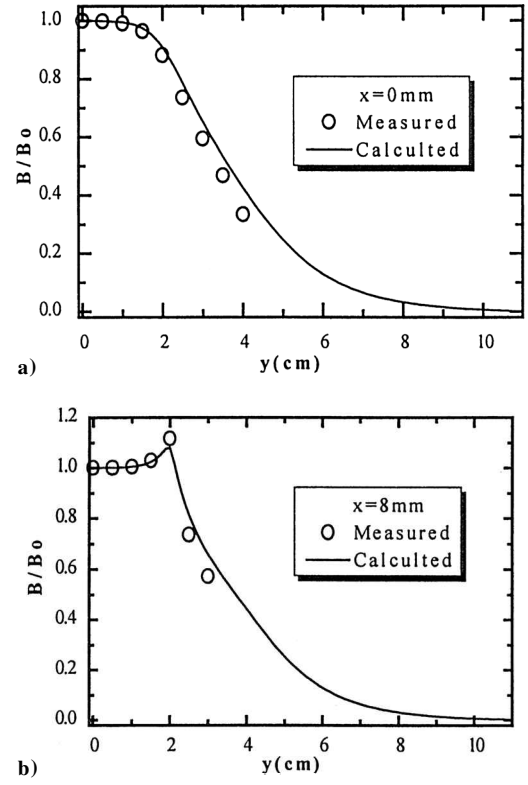

Fig. 3 Spatial distribution of B/B_0.

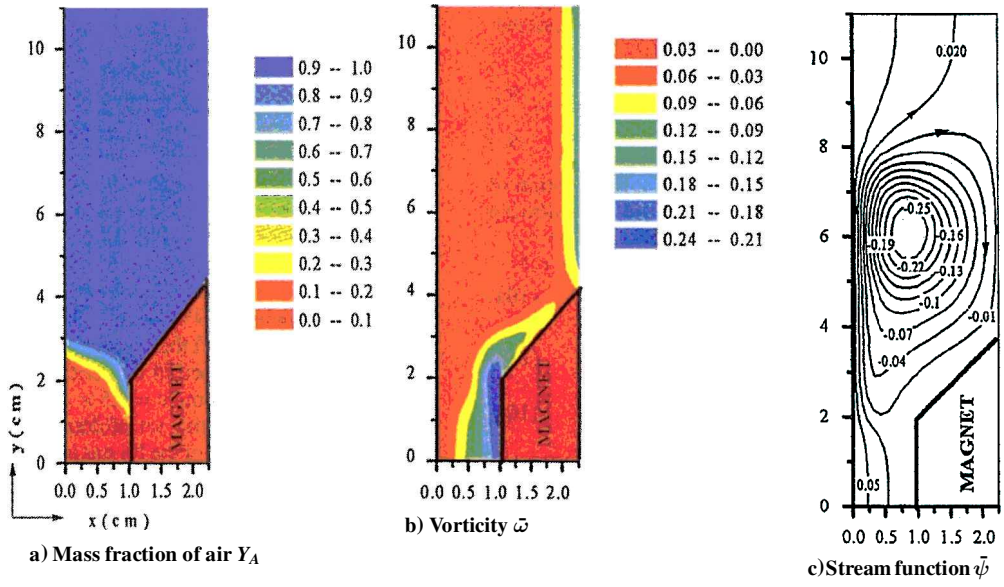

Fig. 4 Spatial distribution under a magnetic field gradient with B_0 = 1.5 T.

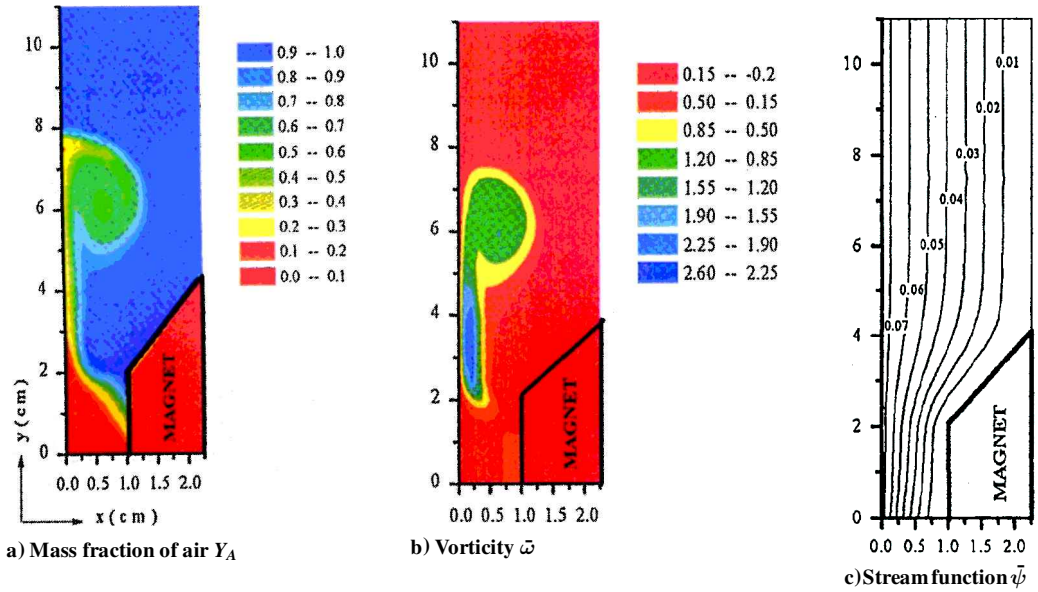

Fig. 5 Spatial distribution in the absence of a magnetic field.

and the oxygen concentration in the gas mixture. This kind of flow does not arise for isothermal single-component gases but occurs in multicomponent gases, where $\boldsymbol{f}_m$ becomes a nonconservative force.

The flowfield represented by the stream function $\bar{\psi}$ in Fig. 4c shows an accelerated N_2 gas jet bordered on both sides by a circulating gas flow that is rotating clockwise to the right of the jet and counterclockwise to the left of the jet. This shows that the air is drawn into the region of higher $\boldsymbol{B}$, and, as a result, the N_2 stream is pushed out toward the weaker field by the air and accelerated.

For comparison, similar numerical simulations were done for no magnetic force, that is, $\bar{f}_m = 0$ in Eq. (10). The results are shown in Fig. 5. In contrast to the results shown in Fig. 4, there is no accelerated N_2 gas flow, and no vorticity or recirculating flows are generated. These flow patterns are similar to that shown in Fig. 1b. Comparison between Figs. 4 and 5 shows that the magnetic field has a significant effect on the gas flows.

Figure 6 shows the velocity distribution for the magnetically induced gas jet along the central y axis (solid line). The maximum velocity of the jet, $u_{\max} = 44$ cm/s, near $y = 3.5$ cm when the entrance velocity of the N_2 gas jet was 7.4 cm/s and $B_0 = 1.5$ T. The velocity distribution in the absence of a magnetic field is also represented in Fig. 6. This also clearly indicates the effect of the magnetic field gradient on the jet's velocity distribution.

In these calculations, we neglected gravitational buoyancy forces in Eq. (10a). The simulation results in the presence of gravitational buoyancy are also shown by dashed lines in Fig. 6. The maximum velocity of the jet, $u_{\max} = 46$ cm/s, near $y = 3.9$ cm when $B_0 = 1.5$ T. The effect of gravitational buoyancy is considered small in the presence of magnetic field of 1.5 T, whereas it affects nitrogen gas flow in the absence of the magnetic field ($u_{\max} = 8.3$ cm/s). Furthermore, the same magnetic phenomenon was observed when N_2 gas was injected horizontally. Because of the preceding discussions, we neglected gravitational buoyancy to estimate the effect of magnetic force.

A similar simulation was made by varying B_0, as shown in Table 1. The dependence of u at $y = 3$ cm on B_0 is shown in Fig. 7 and is found to increase with B_0.

IV. Measurement of Velocity

For comparison with our numerical simulations, we measured the velocity profile of the N_2 gas jet under the same conditions. We measured the velocity of gas jet at $y = 3$ cm and as a function of B_0. Figure 7 shows that the measured velocity (○) increases

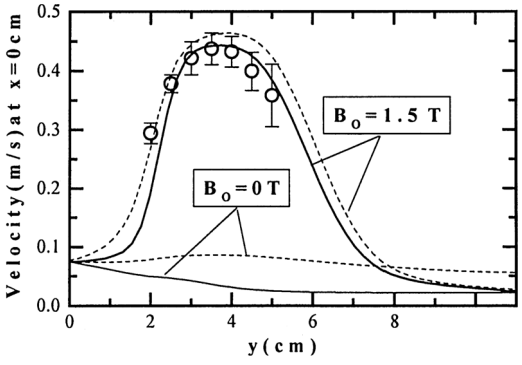

Fig. 6 Distribution of N_2 gas velocity along the y axis with and without the $B_0 = 1.5$ T: ——, simulated results in the absence of gravitational buoyancy; – – –, simulated results in the presence of gravitational buoyancy; and ○, measured velocity profile.

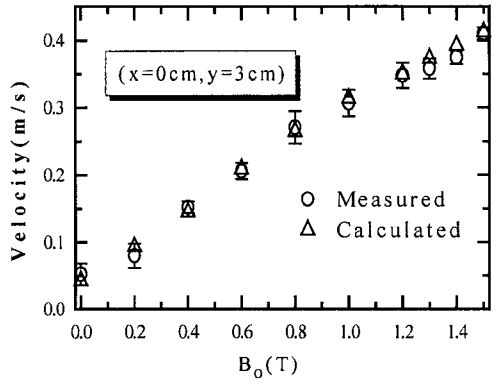

Fig. 7 Velocity of N_2 gas jet ($y = 3$ cm) vs B_0.

approximately linearly with B_0. This relationship is also found by the numerical simulations (see Sec. III.D). Thus, the experimental results agreed well with the simulated values.

We also measured the spatial distribution of velocity along the y axis when $B_0 = 1.5$ T (○ in Fig. 6). When $y < 3$ cm, the velocity increases with increasing y and takes the maximum value, 44 cm/s in the range of $3 < y < 4$ cm. At $y = 4.5$ cm, $u = 39$ cm/s. Figure 6 shows that the measured and simulated velocities agree within experimental errors. Thus, the close agreement between the experimental and simulated values validates the physical model of magnetoaerodynamics and also certifies the accuracy of our numerical simulations.

The present study suggests a new method to accelerate or ventilate gas flows without a fan or a chimney. For example, when $B_0 =$ 1.0 T, N_2 gas is accelerated up to 30 cm/s in Fig. 7.

These magnetically induced gas flows affect combustion in diffusion flames because combustion always causes a decrease of ρ, Y_{O_2}, and $\chi_{O_2}(T)$ and diffusion flames behave like an N_2 gas stream under magnetic field gradients. In fact, magnetic promotion of combustion in diffusion flames has been demonstrated.[6] Therefore, this study suggests the potential use of magnetic attractive forces acting on O_2 gas to control gas flows and combustion. Magnetic fields on the order of 1 T can be easily achieved by using recently developed strong permanent magnets (e.g., Fe–B–Nd compounds). These magnets will make the application of magnetoaerodynamics possible.

V. Conclusions

In MHD, Lorentz force, the third term of Eq. (1), plays an important role. On the other hand, in magnetoaerodynamics, magnetostriction force, the first and second terms of Eq. (1), contributes to induce gas flows. In this paper, the behavior of gas flows in the presence of a magnetic field, especially an N_2–air jet, has been analyzed numerically to clarify the mechanism quantitatively.

The key results from this work are as follows:

1) The magnetic body force acting on a gas mixture containing PM O_2 gas, which can be represented as

$$f_m = \tfrac{1}{2}\mu_0 \chi_{O_2}(T)\rho Y_{O_2} \nabla H^2$$

becomes nonconservative under the gradients of both the O_2 concentration and the magnetic field strength.

2) The numerical analyses clarify the mechanism of the coupling between magnetic forces and the convective motion and indicate the existence of convective flows of the gas mixtures due to the nonconservative magnetic body force.

3) Simulations showed that the maximum velocity of N_2 gas, u_{max}, increases with an increase in the magnetic field strength (B_0). For $B_0 = 1.5$ T and an entrance velocity of the N_2 gas of 7.4 cm/s, $u_{max} = 44$ cm/s. Numerical results agree well with the experimental results.

4) This study suggests the potential use of the attractive magnetic force acting on paramagnetic O_2 gas to control gas flows and combustion.

Acknowledgments

The authors thank the Agency of Industrial Science and Technology for the use of the Research Information Processing System/Station M1900/20 computer. They also thank Core Research for Evolutional Science and Technology and the Japanese Science and Technology Corporation for part of the funding.

References

[1]Chandrasekhar, S., *Hydrodynamic and Hydromagnetic Stability*, Dover, New York, 1981, Chaps. 4, 5, and 9.

[2]Wakayama, N. I., "Behavior of Gas Flow Under Gradient Magnetic Fields," *Journal of Applied Physics*, Vol. 69, No. 4, 1991, pp. 2734–2736.

[3]Herzberg, G., *Molecular Spectra and Molecular Structure I. Spectra of Diatomic Molecules*, Van Nostrand Reinhold, New York, 1939, pp. 366, 462.

[4]Chemical Society of Japan (ed.), *Kagakubinran (Tables of Physical and Chemical Data)*, 2nd ed., Maruzen, Tokyo, 1975, p. 1253.

[5]Wakayama, N. I., "Effect of a Decreasing Magnetic Field on the Flow of Nitrogen Gas," *Chemical Physics Letters*, Vol. 185, No. 5–6, 1991, pp. 449–451.

[6]Wakayama, N. I., "Magnetic Promotion of Combustion in Diffusion Flames," *Combustion and Flame*, Vol. 93, No. 3, 1993, pp. 207–214.

[7]Wakayama, N. I., Ito, H., Kuroda, Y., Fujita, O., and Ito, K., "Magnetic Support of Combustion in Diffusion Flames Under Microgravity," *Combustion and Flame*, Vol. 107, No. 1–2, 1996, pp. 187–192.

[8]Ross, H. D., Sotos, R. G., and Lockwood, F. C., "Observations of Candle Flames Under Various Atmospheres in Microgravity," *Combustion Science and Technology*, Vol. 75, No. 1–3, 1991, p. 155.

[9]Landau, C. P., and Lifshitz, E. M., *Electrodynamics of Continuous Media*, Pergamon, Oxford, 1960, Chap. 4.

[10]Stratton, J. A., *Electromagnetic Theory*, McGraw–Hill, New York, 1941, p. 153.

[11]Yabe, A., and Maki, H., "Augmentation of Convective and Boiling Heat Transfer by Applying an Electro-Hydrodynamic Liquid Jet," *International Journal of Heat and Mass Transfer*, Vol. 31, No. 2, 1988, pp. 407–417.

[12]Kittel, C., *Introduction to Solid State Physics*, 2nd ed., Wiley, New York, 1956, Chap. 9.

[13]Williams, F. A., *Combustion Theory*, Benjamin/Cummings, Menlo Park, CA, 1985, p. 2.

[14]Society of Mechanical Engineers (ed.), *Fundamentals of Computational Fluid Dynamics*, 4th ed., Corona, Tokyo, 1990, p. 71.

S. K. Aggarwal
Associate Editor